Université Paris-Sud

Ecole Doctorale Particules Noyau Cosmos
Laboratoire de structure du nucléon au CEA/Irfu/SPhN

Discipline : Physique

Thèse de doctorat

Soutenue le 25 juin 2015 par

Maxime DEFURNE

Photon and π^0 electroproduction at Jefferson Laboratory - Hall A

Directeur de thèse :	Franck Sabatié	Docteur (CEA/Irfu/SPhN/LSN)
Composition du jury :		
Président du jury :	Etienne Augé	Professeur (Université Paris Sud)
Rapporteurs :	Zein-Eddine Meziani	Professeur (Temple University)
	Paul Stoler	Professeur (Rensselaer Polytechnic Institute)
Examinateurs :	Gunar Schnell	Professeur (University of the Basque Country)
	Peter Kroll	Professeur (Bergische Universität Wuppertal)
	Carlos Muñoz Camacho	Docteur (IPN Orsay)

July 1, 2015

Contents

Acknowledgements

First I would like to express my endless gratitude to my PhD supervisor Franck Sabatié for his trust, his advices and his support. I will keep working hard to become an expert as accomplished as he is, on both human and scientific aspects. Thank you also for reminding to take vacations when I needed some.

I have spent three years with the amazing people of the former group CLAS in the *Service de physique nucléaire* (SPhN) at CEA-Saclay. This work could not have been as rich as it is without all the members of the group: I am not only talking about the carbohydrate intake that represent the numerous cakes we shared, but also all the discussions about experimental and theoretical aspects. Thank you Hervé Moutarde (undoubtly the head pastry chef of the group) and Adrien Besse for the patience and the clarifications in explaining me the QCD theory in hadronic physics. Thank you Sébastien Procureur, Gabriel Charles, Simon Bouteille and Maxence Vandenbroucke for this discussions about detectors but also for some mémorable table tennis games (keep training hard Gabriel). In advance, thank you Bryan Berthou for the future advices you will provide me in structuring the analysis code of the CLAS12 DVCS experiment. Finally I want to thank Jacques Ball and Michel Garçon. I have learnt so much from them.

I acknowledge all the members of SPhN. Particularly I want to thank the always-smiling head of the division, Héloïse Goutte, for welcoming me during my PhD. I am also grateful to Danielle Coret and Isabelle Richard, making everything so much easier in the division. Finally a special thanks to my friend Eric Fuchey for all his strong help and support here at Saclay but also back at Jefferson Laboratory during my internship.

My gratitude also goes to the members of the Hall A DVCS collaboration. Special thanks to Carlos Muñoz Camacho and Charles Hyde with whom we spent hours debatting on data analysis, radiative corrections and many more analysis details. It was a great pleasure for me working with you. Finally I would have never heard about generalized parton distributions and deeply virtual Compton scattering without Alexandre Camsonne who made me discover Jefferson Laboratory, the Hall A, hadronic physics, the best restaurants in Newport News, and so on.

I would like to thank all the members of the examination committee. Special thanks to Paul Stoler and Zein-Eddine Meaziani for their careful reading of the manuscript.

On the personal side, I thank my friends Benoit Latour, Jordane Soussi and Patrick Hsia for encouraging me all along these years. I enjoyed our reflections about how to change the world. A special thanks to my friends Cédric Mezrag and Laetitia Leduc who helped me getting ready for the most important interview of my life. I have appreciated a lot watching a good old *Doctor Who* episode before this "D-Day" in order to relax. Since I was born, my family supports me and I would have never reached this far without them. I thank them for having been there at anytime. Finally I want to dedicate the last sentences to my lovely girlfriend. Although the last months were very difficult, she was there, helping me to give the best of myself. Thank you for your patience, kindness and love. We finally did it!

Introduction

The deepest desire of mankind[1] has always been to understand the universe. A significant step toward this undertanding will be achieved when the following question is answered: *What is it made of ?* Since the ancient greeks and the four elements, a lot have been learnt about the structure of matter. It appears to be built with a finite set of elementary particles, connected through four interactions which are described by the Standard Model. Whereas the Large Hadron Collider keeps challenging the predictions of the Standard Model at higher and higher energies, we are still far from completely understanding how these elementary blocks organize themselves in a proton.

Indeed, in the late 1960s, DIS measurements at SLAC confirmed that the proton is a composite object made of quarks and gluons. These particles interact through the strong interaction. At high energy, the strong interaction can be computed using perturbative quantum chromodynamics (QCD), the associated field theory. Indeed the coupling constant becomes small and quarks behave as if they were free. It is the so-called *asymptotic freedom*. Nevertheless, at long distance (typically the proton size), the coupling constant becomes large and perturbation theory cannot be applied anymore. In other words, despite the promising ways of non-perturbative calculations (Schwinger-Dyson equations, lattice QCD,...), the structure of the hadrons cannot be accessed through calculations yet.

Pieces of information about the nucleon structure have been revealed by scattering experiments. Indeed scattering processes can be split into two parts:

- A hard part/short distance part calculable perturbatively.
- A soft part describing the interaction with the nucleon medium. This part encodes the nucleon structure.

This splitting method is called *factorization*. As a consequence the scattering cross section is parametrized by functions associated to the soft part. From the cross section measurement, we derive these functions and get some insight about the structure of the hadron. For instance form factors and parton distribution functions, related to spatial and momentum distributions, have been studied using elastic and deep inelastic scattering. Unfortunately, it is not enough to explain the confinement of the quarks inside hadrons, the proton mass and spin.

In the mid 90's, new kinds of distributions called *generalized parton distributions* are defined. They represent a higher level of information than FFs and PDFs since they encapsulate both spatial and momentum information. Using the GPDs, we could derive the total orbital angular momentum of quarks thanks to Ji's sum rule. Experimentally they are related to deep exclusive processes. A worldwide experimental program has been dedicated to study such processes. This thesis deals in particular with two experiments measuring cross sections of photon and π^0 electroproduction in order to determine the GPDs. The thesis is articulated as follows:

[1] It is maybe more exact to say one of the deepest desires.

- Chapter 1 introduces the theoretical framework of GPDs and how they are involved in the cross sections of interest. We discuss also GPD models and the existing experimental data.
- Chapter 2 is dedicated to the description of Jefferson Lab, Hall A of Jefferson Lab and the experimental setup.
- Chapter 3 focuses on the extraction of the DIS cross section in order to perform a quality check of our data set. It allows us to develop a method for cross section extraction.
- Chapter 4 is about the data analysis of the E00-110 experiment. All the cuts and corresponding corrections are presented.
- Chapter 5 is subdivided into three parts: It presents the radiative corrections and the Monte-Carlo simulation used for acceptance computation. In the last part, we explain the fitting procedure employed to extract DVCS cross sections and effective CFFs.
- Chapter 6 summarizes the results on photon electroproduction and compares them to predictions from different GPD-based models.
- Finally Chapter 7 is a condensate of chapters 4,5 and 6 applied on the π^0 analysis. The results of the first Rosenbluth separation performed on the π^0 electroproduction cross section are commented on and compared to two GPD models. A careful study of systematic errors has been carried out.

Chapter 1

Nucleon structure through deep exclusive processes

One of the hints that the proton has an internal structure were obtained by studying elastic scattering off the proton in the late 1950's at Stanford university by Hofstadter and his team. The corresponding cross section can be parametrized using form factors (FFs), which are related to the spatial distribution of charge in the nucleon (proton and neutron). In the late 1960's at the Standford Linear Accelerator (SLAC), the study of Deep Inelastic Scattering (DIS) confirmed the existence of quarks and that the proton is a composite particle. The parton distribution functions (PDFs) parametrize the DIS cross section and are related to the longitudinal momentum distribution of partons (quark and gluon) in the nucleon. Nevertheless the correlation between both spatial and momentum information cannot be derived from FFs and PDFs. It is only in the mid-90's that was introduced the concept of Generalized Parton Distributions (GPDs) which are a generalization of the FFs and PDFs. GPDs are objects that encapsulate a higher level of information since they actually encode the correlation between momentum and spatial distributions. GPDs obey a set of properties and sum rules from which modelization is possible. These models are then tested by comparing observables measured in deep exclusive processes. In particular we will focus here on Deeply Virtual Compton Scattering (DVCS) and deep π^0 electroproduction. After explaining how GPDs are involved in these processes, we briefly present the current state of the experimental program. Finally we introduce the experiments of interest in this thesis and what new information we want to extract from the data.

1.1 Elastic scattering and form factors

A particle a scatters elastically off a particle b when the final state is only composed of particles a and b. Figure 1.1 shows a diagram of elastic scattering. We note:

- $k_i = (\mathbf{k_i}, E)$ the 4-momentum of the incident electron.
- $k_f = (\mathbf{k_f}, E')$ the 4-momentum of the scattered electron.
- θ_e the scattering angle in the lab frame.
- $q = k_i - k_f$ the 4-momentum of the virtual photon and $Q^2 = -(k_f - k_i)^2$ its virtuality.

In 1911, Rutherford studied the scattering of alpha particles off a gold foil [1]. Assuming a point-like target with no recoil and a non-relativistic scattered particle, the cross section

is given by:

$$\left(\frac{d\sigma}{d\Omega}\right)_{Rutherford} = \frac{\alpha}{16E^2 \sin^4\left(\frac{\theta_e}{2}\right)}, \tag{1.1}$$

where α is the fine-structure constant. If one uses relativistic electrons instead of α-particles, the cross section reads:

$$\left(\frac{d\sigma}{d\Omega}\right)_{Mott} = \frac{\alpha}{4E^2 \sin^4\left(\frac{\theta_e}{2}\right)} \cos^2\left(\frac{\theta_e}{2}\right), \tag{1.2}$$

but the experimental cross section deviated from this formula. If the target is an extended object, the electron cross section is modified and becomes:

$$\frac{d\sigma}{d\Omega} = \left(\frac{d\sigma}{d\Omega}\right)_{Mott} |F(\Delta)|^2, \tag{1.3}$$

with $\Delta = p - p'$ and $F(\Delta)$ the form factor. $F(\Delta)$ is the Fourier transform of the transverse spatial distribution of charge $\rho(r)$:

$$F(\Delta) = \int \rho(r) e^{i\Delta r} dr^3. \tag{1.4}$$

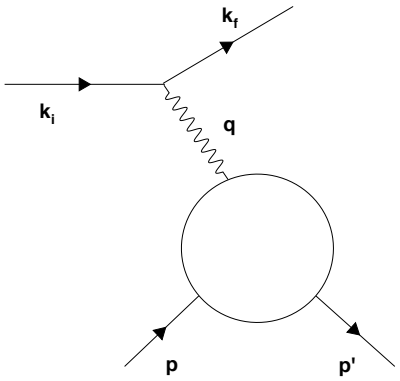

Figure 1.1: Elastic scattering diagram. Note that in the case of elastic scattering, $\Delta = -q$.

Following the steps of Rutherford, Robert Hofstadter studied the nucleon structure using elastic scattering $ep \to e'p'$ at SLAC between 1954 and 1957. His work was awarded the Nobel prize in 1961. In the nucleon case, the cross section can be parametrized by two structure functions called the Sachs form factors G_E and G_M. The cross section is written [2]:

$$\frac{d\sigma}{d\Omega} = \frac{\alpha}{4E^2 \sin^4\left(\frac{\theta_e}{2}\right)} \frac{E'}{E} \left[\frac{G_E^2(\Delta^2) + \tau G_M^2(\Delta^2)}{1+\tau} \cos^2\left(\frac{\theta_e}{2}\right) + 2\tau G_M^2(\Delta^2) \sin^2\left(\frac{\theta_e}{2}\right)\right], \tag{1.5}$$

with $\tau = \frac{-\Delta^2}{4M^2}$ and M the mass of the proton. By measuring the cross section at the same Δ^2 but two different beam energies, it is possible to extract G_E and G_M. This way of separating the two FFs using different beam energies is called a *Rosenbluth separation*. Later in this chapter, we will use the Pauli and Dirac FFs defined as:

$$F_1(Q^2) = \frac{G_E(Q^2) + \tau G_M(Q^2)}{2\tau} \tag{1.6}$$

$$F_2(Q^2) = \frac{G_M(Q^2) - G_E(Q^2)}{1+\tau} \tag{1.7}$$

In the Breit frame in which the initial and final proton momenta have the same magnitude but opposite directions, G_E and G_M are the Fourier transform of the charge and magnetic distributions of the proton. The proton charge radius can be derived from the knowledge of G_E using the formula:

$$\langle r_E^2 \rangle = -\frac{6}{G_E(0)} \frac{dG_E(Q^2)}{dQ^2}\bigg|_{Q^2=0}. \tag{1.8}$$

Applying Eq. 1.8, a charge radius of $r_p = \langle r_E^2 \rangle = 0.879(8)$ fm was derived by extrapolating G_E-measurements performed at low Q^2 [3]. This result is in good agreement with the radius provided by the study of the Lamb shift and the hyperfine structure of electronic hydrogen atoms [4], giving $r_p = 0.8768(69)$ fm. Nonetheless, recent studies of muonic hydrogen's Lamb shift [5] gave $r_p = 0.84184(67)$ fm, at 7-σ from the value given by the electronic measurements. This discrepancy has not been understood yet.

1.2 Deep inelastic scattering and parton distribution functions

Let us now consider the inelastic reaction $ep \to eX$. We define two additional variables:

- The Bjorken variable $x_B = \frac{Q^2}{2M\nu}$, where $\nu = E - E'$.
- $W^2 = (p+q)^2 = M^2 + Q^2\left(\frac{1}{x_B} - 1\right)$ the invariant mass of the hadronic final state.

The deep inelastic regime is defined by $W \gg M$ and $Q^2 \gg M^2$. In this regime, the final state is composed of more particles than the initial state. Under the one-photon exchange assumption, the DIS cross section is given by the contraction of the leptonic and hadronic tensors. The information about the proton is encapsulated in the hadronic tensor. In the case of unpolarized DIS, once symmetries and invariances have been applied, the hadronic tensor can be parametrized by two dimensionless structure functions depending on Q^2 and x_B. As a consequence the cross section is related to these two functions by:

$$\frac{d\sigma}{d\Omega dE'} = \left(\frac{d\sigma}{d\Omega}\right)_{Mott} \left[\frac{F_2(x_B, Q^2)}{\nu} + \frac{2}{M} F_1(x_B, Q^2) \tan^2\left(\frac{\theta_e}{2}\right)\right], \tag{1.9}$$

In the late 1960's at SLAC, Friedman, Kendall and Taylor performed DIS cross section measurements at several Q^2 [6] [7]and were later awarded the Nobel Prize in 1990. From these measurements they noticed first that F_2 was independent of Q^2, as if the electron was scattering off point-like particles. Moreover F_1 and F_2 were related through the Callan-Gross relation, indicating that these particles were fermions:

$$F_2(x_B) = 2x_B F_1(x_B)\ . \tag{1.10}$$

These results validated the theory of Gell-Mann [8] (Nobel Prize 1969) and Zweig [9] in 1964 that the proton was composed of quarks and gluons. Richard Feynman (Nobel Prize 1965) developed the parton model in 1969: In the limit $Q^2 \to \infty$ and $\nu \to \infty$ but fixed x_B (Bjorken limit), the virtual photon interacts with a single quark in the proton (Figure 1.2). Within this model, F_2 is related to the so-called parton distribution functions (PDFs).

$$F_2(x_B) = x_B \sum_f e_f q_f(x_B), \tag{1.11}$$

where e_f stands for the quark electric charge in units of the positron charge and q_f the PDF for a quark of flavor f.

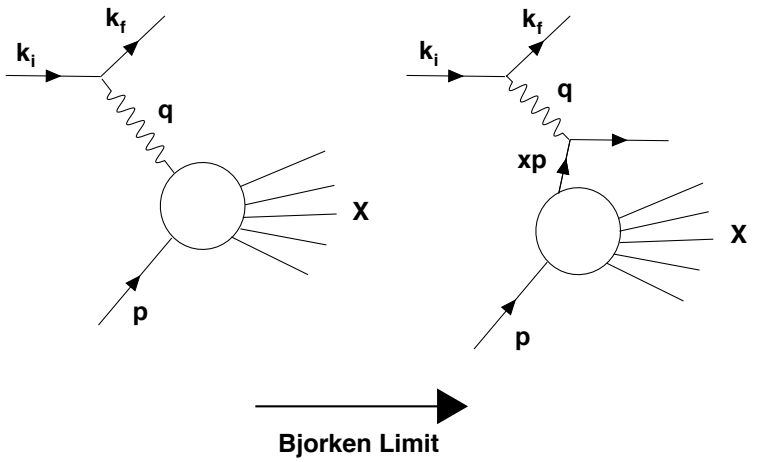

Figure 1.2: Deep inelastic scattering. In the Bjorken limit, the photon interacts with a single quark.

In the infinite momentum frame, where the proton speed is close to the speed of light along the z-axis colliding head-on with the virtual photon, x_B represents the fraction of momentum carried by the struck quark. In this frame $q_f(x_B)$ can be interpreted as the probability to find a parton with flavor f carrying a fraction x_B of the proton momentum. Since the time scale of the interaction between two partons is much greater than the one between the photon and the active quark, the DIS cross section can be rewritten as the product of the probability to find a quark and the probability to scatter off this quark:

$$\frac{d^2\sigma_{DIS}}{dx_B dQ^2} = \sum_f q_f(x_B) \times \frac{d^2\sigma_{eq\to eq}}{dx_B dQ^2}, \tag{1.12}$$

$$= \sum_f q_f(x_B) \times e_f^2 \frac{2\pi\alpha^2}{Q^4}\left[1 + \left(1 - \frac{Q^2}{x_B s}\right)\right], \tag{1.13}$$

where $s = (p + k_i)^2$. Through this factorized form, the parton model infers the notion of *asymptotic freedom*: At high Q^2 and therefore small resolved distance, the reaction occurs as if the electron scatters off a free quark.

By extracting F_2 over a larger kinematic domain, the experimentalists noticed that the scaling becomes violated when moving away from the x_B value of first SLAC measurements. The scaling violation is explained by the active quark emitting gluons (see Figure 1.3), in other words by QCD radiative corrections. The Q^2-evolution of PDFs is driven by the DGLAP (Dokshitzer, Gribov, Lipatov, Altarelli and Parisi) equations, resulting in a logarithmic Q^2-dependence of the PDFs.

1.3 Generalized parton distributions

The FFs and PDFs give information on either the position or the momentum fraction of the parton in the nucleon, but do not correlate both information. In the quest of understanding nucleon structure, theorists have been looking for distributions containing the most information and related to experimental observables. We are going to define the GPDs starting from

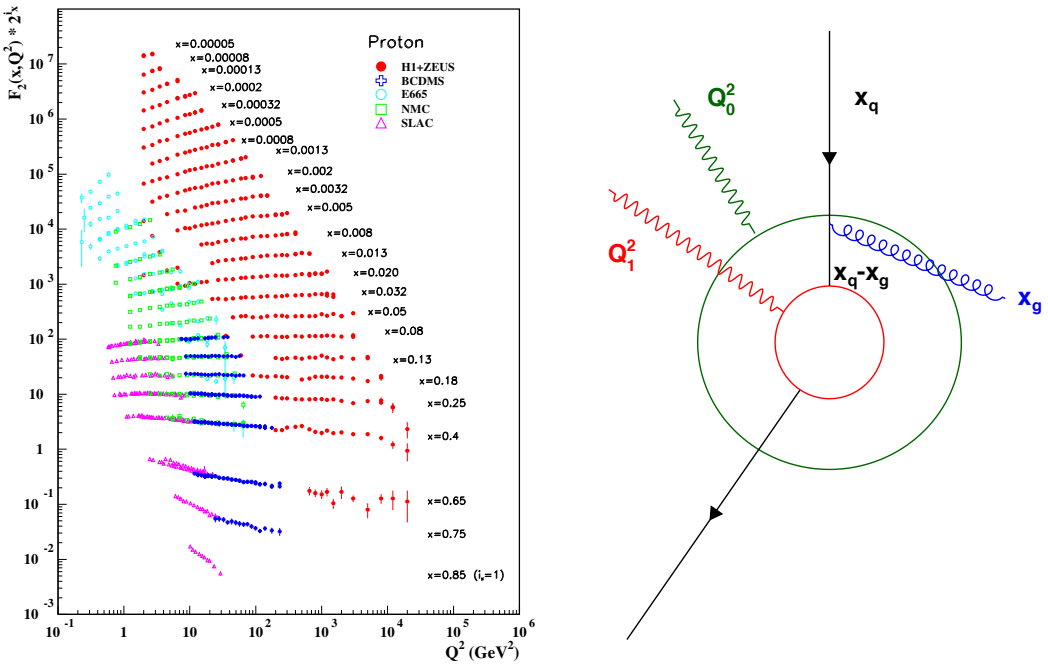

Figure 1.3: Left: F_2 measured at different x_B and Q^2. There is an apparent scaling at $x_B \sim 0.2$ where SLAC performed their first measurements. Right: The green virtual photon interacts with a quark with a momentum fraction x_q. At $Q_1^2 > Q_0^2$, the red virtual photon resolves smaller distances and interact with a quark $x_q - x_g$ which has emitted previously a gluon. As a consequence, when going at higher Q^2, the quark PDF decreases for $x_B > 0.2$ and increases below. The gluon PDFs also increases with Q^2.

the Wigner distributions. Then we will describe their support and several of their properties which may be used to constrain models. At the end of this section, we will present the double distributions which are convenient ways to build a GPD model given their properties.

1.3.1 From Wigner distributions to generalized parton distributions

In 1932, Wigner (Nobel Prize 1963) defined a new kind of distribution which is a function of both spatial and momentum coordinates. Taking a wave function $\psi(r)$, Wigner defined the following distribution:

$$P(r,k) = \int_{-\infty}^{+\infty} dz e^{ikz} \psi^*(r - z/2)\psi(r + z/2) \, . \tag{1.14}$$

The spatial distribution is recovered by simply integrating the Wigner distribution over the momentum variables. Inversely, we integrate over the spatial variables to recover the momentum distribution. Adapting this formalism in quantum field theory, we first define the Wigner operators:

$$\mathcal{W}_\Gamma^f(r,k) = \int d^4z e^{ik\cdot z} \bar{\Psi}^f \left(r - \frac{z}{2}\right) \Gamma \mathcal{L} \Psi^f \left(r + \frac{z}{2}\right), \tag{1.15}$$

where r is the space-time coordinates of the quark with flavor f, k being the associated 4-momentum and Ψ its field. Γ is a Dirac operator. $\mathcal{L}$ is a Wilson line which ensures the gauge invariance.

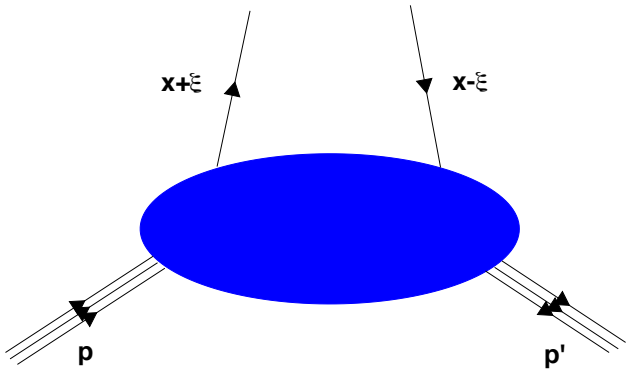

Figure 1.4: Diagram associated to the matrix element F^f_Γ.

From the Wigner operators, the Wigner distributions are given by:

$$W^f_\Gamma(r,k) = \frac{1}{2M}\int \frac{d^4q}{(2\pi)^4}\left\langle p'\left|\mathcal{W}^f_\Gamma(r,k)\right|p\right\rangle, \tag{1.16}$$

where p and p' are the inital and final momenta of a proton, with $q = p' - p$. The Wigner distributions encapsulate all the information about the momentum and spatial distributions of partons, including their correlations. In the infinite momentum frame where the proton moves along the z-axis, the interacting parton is mainly on the light cone + component (see Appendix C for definitions). Therefore the k^- and $k_\perp$ components are very small and difficult to access. By integrating over k^- and both components of $k_\perp$ and chosing a light cone gauge, we obtain the so called generalized parton distributions (GPDs):

$$F^f_\Gamma(x,\xi,t) = \frac{P^+}{4\pi}\int dz^- e^{ixP^+z^-}\langle p'|\bar{\Psi}_q\left(-\frac{z}{2}\right)\Gamma\Psi_q\left(\frac{z}{2}\right)|p\rangle\Big|_{z^+=\vec{z}_\perp=0}. \tag{1.17}$$

The GPDs F^f_Γ are associated to the diagram illustrated by the Figure 1.4: x is the average longitudinal momentum fraction carried by the active quark, -2ξ the longitudinal momentum transfer and P the sum $p+p'$. ξ is approximately given by $\frac{x_B}{2-x_B}$. t is the squared momentum transfer to the proton $|p-p'|^2$. Note that, in the case of GPDs and PDFs, the Wilson line reduces to unity when chosing a light-cone gauge.

Taking $\Gamma = \gamma^+$ or $\Gamma = \gamma^+\gamma_5$, we obtain the chiral-even GPDs (same helicity for the emitted and reabsorbed parton):

$$F^f_{\gamma^+}(x,\xi,t) = H^f(x,\xi,t)\bar{N}(p')\gamma^+N(p) + E^f(x,\xi,t)\bar{N}(p')\sigma^{+\nu}\frac{\Delta_\nu}{2M}N(p), \tag{1.18}$$

$$F^f_{\gamma^+\gamma_5}(x,\xi,t) = \tilde{H}^f(x,\xi,t)\bar{N}(p')\gamma^+\gamma_5N(p) + \tilde{E}^f(x,\xi,t)\bar{N}(p')\gamma_5\frac{\Delta^+}{2M}N(p), \tag{1.19}$$

The correlator with $\Gamma = \sigma^{+\perp}\gamma_5$ is parametrized by four chiral-odd GPDs called also transversity GPDs H_T, $\tilde{H}_T$, E_T and $\tilde{E}_T$. Unlike E-GPDs, H-GPDs are not sensitive to the parton helicities. When they are tilded, GPDs are involved in processes with a flip of the nucleon helicity. The variables x and ξ evolve between [-1 ; 1]. By comparing x and ξ, we may interpret the process in different ways:

- For $x < -\xi$ an antiquark exits and is reabsorbed in the nucleon. Same thing with a quark for $x > \xi$. These two regions are called the DGLAP regions since the GPDs evolve in this region like the PDFs, *i.e.* according to the DGLAP equations.
- For $-\xi < x < \xi$: the nucleon emits a quark-antiquark pair. This region is called the ERBL (Efremov, Radyushkin, Brodsky and Lepage) region.

1.3.2 Properties of GPDs

The chiral-even GPDs are generalizations of PDFs and FFs just by looking at their associated correlator. Indeed, for a flavor f, we have when the squared momentum transfer to the proton $t \to 0$:

$$H^f(x,0,0) = q_f(x), \tag{1.20}$$
$$\tilde{H}^f(x,0,0) = \Delta q_f(x)\ . \tag{1.21}$$

Moreover the elastic form factors are obtained from the first moment of the corresponding GPDs:

$$\int_{-1}^{1} H^f(x,\xi,t)\ dx = F_1^f(t) \qquad \forall\xi, \tag{1.22}$$
$$\int_{-1}^{1} E^f(x,\xi,t)\ dx = F_2^f(t) \qquad \forall\xi, \tag{1.23}$$
$$\int_{-1}^{1} \tilde{H}^f(x,\xi,t)\ dx = G_A^f(t) \qquad \forall\xi, \tag{1.24}$$
$$\int_{-1}^{1} \tilde{E}^f(x,\xi,t)\ dx = G_p^f(t) \qquad \forall\xi\ . \tag{1.25}$$

Finally the total angular momentum of quark J^f can be accessed through Ji's sum rule [10, 11]:

$$\int_{-1}^{1} x\left[H^f(x,\xi,0) + E^f(x,\xi,0)\right]\ dx = J^f\ \forall\xi\ . \tag{1.26}$$

The chiral-odd GPDs are almost unknown compared to the chiral-even GPDs from the experimental and theoretical points of view. Although the chiral-odd GPDs also describe the nucleon structure, they are more difficult to interpret. No model-independent relations with orbital angular momentum of quarks involves the transversity GPDs. The only existing constraint is the forward limit of H_T.

$$H_T^f(x,0,0) = \delta_T q_f(x), \tag{1.27}$$

where $\delta_T q_f(x)$ is the transversity distribution function. In a transversely polarized proton, $\delta_T q_f(x)$ represents the difference between the densities of partons with parallel and antiparallel spins with respect to the proton spin. The chiral-odd GPDs might be necessary to describe several exclusive processes, especially pseudo-scalar meson production.

We finish this exhaustive list of GPD properties with the polynomiality. This property states that the n^{th} moment of GPDs is an even polynomial in ξ.

$$\text{if n even}: \int_{-1}^{1} dx x^n H(x,\xi,t) = a_0 + a_2\xi^2 + a_4\xi^4 + \cdots + a_n\xi^n\ , \tag{1.28}$$
$$\text{if n odd}: \int_{-1}^{1} dx x^n H(x,\xi,t) = a_0 + a_2\xi^2 + a_4\xi^4 + \cdots + a_{n+1}\xi^{n+1}\ . \tag{1.29}$$

Note that the coefficients a_i depend on t. The same property applies to E, $\tilde{H}$ and $\tilde{E}$. The coefficient a_{n+1} of E has the opposite sign of the one of H. In the case of odd n, the highest power is $n-1$ for GPDs $\tilde{H}$ and $\tilde{E}$. Polynomiality is a consequence of the Lorentz invariance.

1.3.3 GPDs and double distributions

Previous properties constrain the GPD models. The polynomiality condition is the most complicated to respect. Nevertheless A. Radyushkin [12, 13] and D. Mueller [14] noticed that the double distributions (DDs) are a convenient way to naturally obey the polynomiality. We first define two variables α and β such that:

$$(x+\xi)P^+ = \beta P^+ - \frac{1}{2}(1+\alpha)\Delta^+, \tag{1.30}$$

where Δ^+ is the longitudinal component of the transferred momentum Δ. α plays the same role as ξ, except that it is not relative to P^+. As $-2\xi = \frac{\Delta^+}{P^+}$, we have $x = \beta + \alpha\xi$. The GPDs is then constructed from the DDs by:

$$GPD^f(x,\xi) = \int_{-1}^{1} d\beta \int_{-1+|\beta|}^{1-|\beta|} d\alpha \delta(x-\beta-\xi\alpha) DD^f(\alpha,\beta), \tag{1.31}$$

The integration boundaries are constrained by x between [-1;1] and ξ between [0;1].

When the momentum transfer $\Delta = 0$, we recover the usual PDF. In the limit $P = 0$ and $\Delta \neq 0$, the matrix element becomes:

$$\langle P+\Delta|\bar{\Psi}_q\left(-\frac{z}{2}\right)\Gamma\Psi_q\left(\frac{z}{2}\right)|P\rangle\big|_{z^+=\vec{z}_\perp=0} \to \langle\Delta|\bar{\Psi}_q\left(-\frac{z}{2}\right)\Gamma\Psi_q\left(\frac{z}{2}\right)|0\rangle\big|_{z^+=\vec{z}_\perp=0}, \tag{1.32}$$

which is a distribution amplitude (DA) representing the probability to produce a meson from a quark-antiquark pair carrying respectively a longitudinal momentum fraction $1+\alpha$ and $1-\alpha$. A. Radyushkin [12, 13] found a profile which respects these two limits:

$$DD(\beta,\alpha) = h(\beta,\alpha)q(\beta), \tag{1.33}$$

$$h(\beta,\alpha) = \frac{\Gamma(2b+2)}{2^{2b+1}\Gamma^2(2b+1)} \frac{[(1-|\beta|)^2-\alpha^2]^b}{(1-|\beta|)^{2b+1}}, \tag{1.34}$$

where $q(\beta)$ is a PDF and $h(\beta,\alpha)$ a profile function allowing to recover a DA when $\alpha \to 0$. The parameter b is a free parameter which tunes the ξ-dependence: when $b \to \infty$, the DD looks like a PDF.

Concerning the t-dependence, it was first included in a factorized manner, *i.e.* such as $H(x,\xi,t) = H_{DD}(x,\xi)F_1(t)$ where $F_1(t)$ is the form factor and $H_{DD}(x,\xi)$ computed with Equation 1.31. Nowadays it is incorporated in the double distribution such as:

$$DD(\beta,\alpha,t) = h(\beta,\alpha)q(\beta) \times \exp\left(p(\beta)t\right) \ , \tag{1.35}$$

where $p(\beta)$ is a profile function. A usual choice is $p(\beta) = a\ln\beta + c$ with a and c parameters but more complex forms exist [15]. Later we will compare our results with several GPD models based on double distributions.

1.4 Deep exclusive processes to access GPDs

GPDs are accessible through the study of deep exclusive processes: they are a rare subset of deep inelastic processes where all particles in the final state are detected as shown in Fig. 1.5.

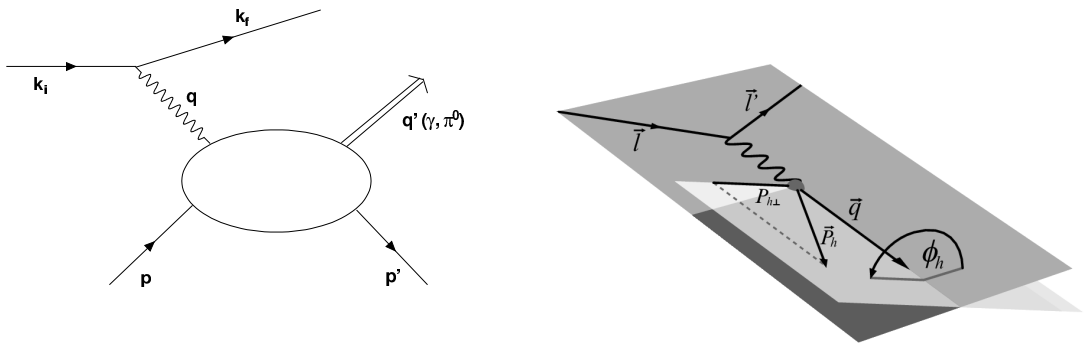

Figure 1.5: Left: Diagram of electroproduction off a proton. Right: Definition of ϕ, the angle between the leptonic and the hadronic plane. On this figure, $P_h = q'$, $l = k_i$ and $l' = k_f$.

We focus on the photon and π^0 electroproduction for which the final state is composed of the scattered electron, the recoil proton and a photon or a π^0.

We define ϕ the angle between the leptonic plane, formed by the scattered electron and the virtual photon, and the hadronic plane defined by the virtual photon and the recoiled proton (Fig. 1.5). We follow the Trento convention [16] defined such as:

$$\cos\phi = \frac{(\mathbf{q}\times\mathbf{k_i})}{|\mathbf{q}\times\mathbf{k_i}|}\cdot\frac{(\mathbf{q}\times\mathbf{q'})}{|\mathbf{q}\times\mathbf{q'}|}\ , \tag{1.36}$$

$$\sin\phi = \frac{(\mathbf{k_i}\times\mathbf{q'})\cdot\mathbf{q}}{|\mathbf{q}\times\mathbf{k_i}||\mathbf{q}\times\mathbf{q'}|}\ , \tag{1.37}$$

The GPDs parametrize the cross sections of deep exclusive processes but in a more involved way than PDFs for DIS. Indeed we have seen that the DIS cross section factorizes into two parts: a term describing the electron-quark scattering and the PDF related to the quark content in the nucleon. GPDs are related to deep exclusive processes based also on the concept of *factorization*. We will sketch the principle of factorization and derive another essential property of the GPDs. Finally we will describe how GPDs enter the photon and π^0 electroproduction cross sections.

1.4.1 Light cone dominance

When computing the amplitude for DVCS (but also DVMP or DIS), we obtain a δ function for momentum conservation involving the 4-momentum of the virtual photon.

$$\delta^4(q) = \frac{1}{(2\pi)^4}\int d^4z e^{iqz}\ . \tag{1.38}$$

Applying the equality 1.38 to this δ function, the amplitude is given as an integral of e^{iqz}. In the proton rest frame, with the z-axis going in the opposite direction with respect to the virtual photon, we have:

$$q = \left(\frac{Q^2}{2Mx_B}, 0, 0, -\frac{Q^2}{2Mx_B}\sqrt{1+4Mx_B/Q^2}\right)\ . \tag{1.39}$$

In the Bjorken limit, Eq. 1.38 gives a non-vanishing result only when:

$$z^- \sim 1/Mx_B\ , \tag{1.40}$$

$$z^+ \sim Mx_B/Q^2\ . \tag{1.41}$$

As causality ensures that $z^2 > 0$, we have $z_\perp < z^- z^+ \sim \frac{1}{Q^2}$. Therefore, in the Bjorken limit, only the space-time regions close to the light cone contribute to the amplitude.

1.4.2 Factorization and twist

The factorization has been proven rigorously at leading-twist for DVCS. In the case of deep virtual meson production, only with longitudinally polarized photon. The following short explanation of factorization is based on DVCS which is the simplest process.

The DVCS amplitude is given by:

$$\mathcal{T}_{DVCS} = i \int d^4 z e^{iqz} \langle p' | T\{j_\mu(z) j_\nu(0)\} | p \rangle, \tag{1.42}$$

with $j_\mu(z)$ the electromagnetic current of quarks defined such as:

$$j_\mu(z) = \sum_f e_f \bar{\Psi}_f(z) \gamma_\mu \Psi_f(z), \tag{1.43}$$

In the Bjorken limit, $z^2 \to 0$ and the correlator of the electromagnetic currents becomes singular. To describe the singularity of the product of operators, Wilson derived the operator product expansion (OPE). It is a Taylor expansion of the product of currents using local operators. Therefore we can write the correlator:

$$T\{j_\mu(z) j_\nu(0)\} \overset{z^2 \to 0}{\sim} \sum_{\tau=2}^{\infty} \sum_{n=0}^{\infty} C_{\tau,n}(z^2) z^{\mu_1} z^{\mu_2} ... z^{\mu_n} \hat{\mathcal{O}}^\tau_{\mu_1 ... \mu_n}(0), \tag{1.44}$$

$\hat{\mathcal{O}}^\tau_{\mu_1 ... \mu_n}(0)$ are a basis of local operators, $z^{(\mu_1} z^{\mu_2} ... z^{\mu_n)}$ traceless homogeneous polynomials. $C_{\tau,n}(z^2)$ are coefficients carrying the singularity. They evolve as:

$$C_{\tau,n}(z^2) \overset{z^2 \to 0}{\sim} \left(\frac{1}{z^2} \right)^{(n - d_\mathcal{O} - 2d_j)/2} \tag{1.45}$$

with $d_\mathcal{O}$ the mass dimension of the operator $\hat{\mathcal{O}}^\tau_{\mu_1 ... \mu_n}$, and n its spin. $\tau = d_\mathcal{O} - n$ is called *twist* and the most important singularities are carried by operators with the minimal twist τ=2. The GPDs introduced in the previous section are associated with the lowest twist operators. The soft part, or the nucleon medium, is described by the operators. The hard/high energy part is given by the coefficients $C_{\tau,n}(z^2)$ which are calculated perturbatively in powers of α_s (Figure 1.7).

To separate the soft part from the hard part, a factorization scale μ_F is introduced. The GPDs and the coefficient describing the hard part depends on it such that the observable is μ_F-independent.

Therefore, the difference between all the exclusive reactions such as DVCS or DVMP lies in the hard scattering kernel, the GPDs being factorized in the soft part. The GPDs are therefore considered *universal*. As a consequence, we can combine the different reactions to get a unified picture of the nucleon.

When $Q^2 \to \infty$, the leading-twist contribution dominates and higher-twist contributions can be safely neglected. In practice, the experiments run at Q^2-values of a few GeV^2 and higher-twist contributions might appear with increasing ratios $\frac{M^2}{Q^2}$ and $\frac{-t}{Q^2}$.

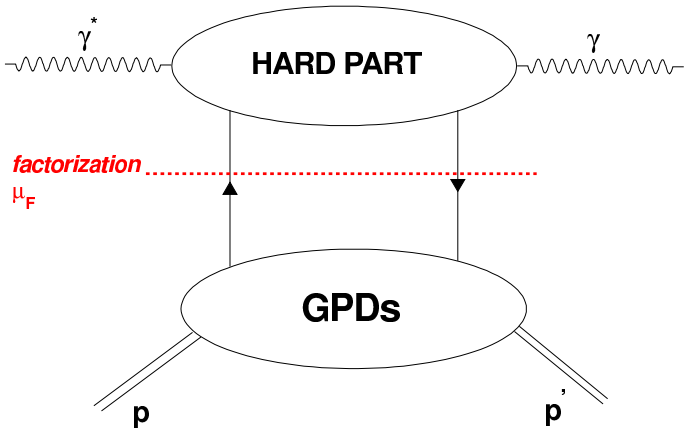

Figure 1.6: The factorization separates a hard scattering kernel computable perturbatively from a low energy part described by the GPDs with respect to a factorization scale μ_F.

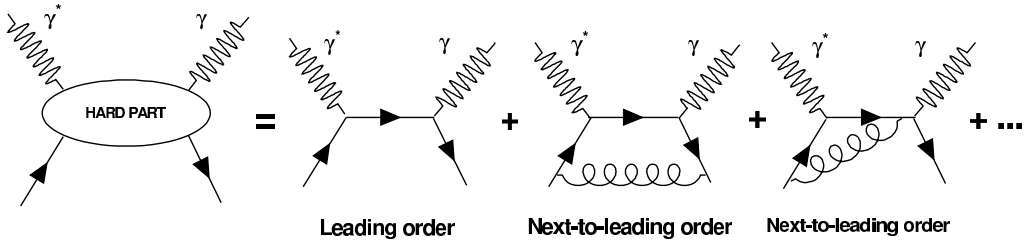

Figure 1.7: The hard scattering kernel is computed perturbatively in α_s.

1.4.3 Deeply virtual Compton scattering

Photon electroproduction arises from the interference of two processes:

- The Bethe-Heitler (BH) process where the photon is emitted by either the incoming or outgoing electrons. In this well-known process, the structure of the nucleon is encoded by the FFs.
- The DVCS process where the photon is emitted by the nucleon. At leading-twist and leading-order, it is described by the handbag diagram (Fig 1.8).

As a consequence, the photon electroproduction cross section reads:

$$\frac{d^5\sigma(\lambda,\pm e)}{dQ^2dx_Bdtd\phi d\phi_e} = \frac{d\sigma_0}{dQ^2dx_B}\frac{1}{e^6}\times\left[\left|\mathcal{T}^{BH}\right|^2+\left|\mathcal{T}^{DVCS}\right|^2\mp\mathcal{I}\right] , \tag{1.46}$$

where $\mathcal{T}_{DVCS}$ is the DVCS amplitude, $\mathcal{T}_{BH}$ the BH amplitude and $\mathcal{I}$ the interference term between the two processes. e is the electron charge, λ the beam helicity. Then we have:

$$\frac{d\sigma_0}{dQ^2dx_B} = \frac{\alpha^3}{16\pi^2(s-M^2)^2x_B}\frac{1}{\sqrt{1+\epsilon^2}} , \tag{1.47}$$

$$\epsilon^2 = 4M^2x_B^2/Q^2 , \tag{1.48}$$

$$s = 2ME + M^2 . \tag{1.49}$$

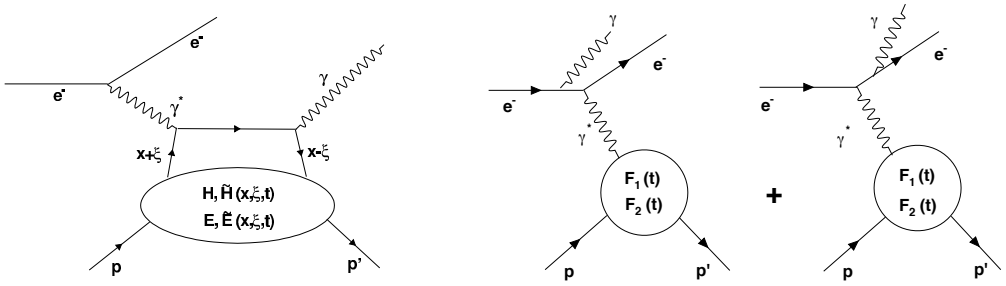

Figure 1.8: On the left, diagram of DVCS at leading-twist, traditionally called handbag diagram. The virtual photon interacts with a single quark inside the nucleon, which then emits a real photon. All vertices in the short distance part are electromagnetic, making the DVCS the golden channel to extract information about GPDs. The two diagrams on the right represents the Bethe-Heitler process with the photon emitted by the electron.

1.4.3.1 Compton Form Factors

The GPDs parametrize the DVCS amplitude but are not directly accessible through the cross section. Indeed, whereas ξ and t are kinematic variables defined by the scattered electron and photon, x is integrated over. The DVCS amplitude is given, at leading-order, by integrals of the form:

$$\int_{-1}^{1}\frac{H(x,\xi,t)}{x-\xi+i\epsilon}dx = \mathcal{P}\int_{-1}^{1}\frac{H(x,\xi,t)}{x-\xi}dx - i\pi H(\xi,\xi,t) , \tag{1.50}$$

where $\frac{1}{x-\xi+i\epsilon}$ is the bare quark propagator. By taking into account the crossed diagram, we define the Compton Form Factors such as:

$$\mathcal{H} = \int_{-1}^{1} H(x,\xi,t)\left(\frac{1}{\xi-x-i\epsilon} - \frac{1}{\xi+x-i\epsilon}\right)dx\ . \tag{1.51}$$

By reducing the integration range from [-1,1] to [0,1] and gathering imaginary and real parts, we define 8 GPD-related quantities directly connected to the DVCS amplitude (same sign conventions for E and $\tilde{E}$):

$$\Re\mathrm{e}\mathcal{H}(\xi,t) = \mathcal{P}\int_0^1 \left[H(x,\xi,t) - H(-x,\xi,t)\right] C^+(x,\xi)dx, \tag{1.52}$$

$$\Im\mathrm{m}\mathcal{H}(\xi,t) = \pi\left(H(\xi,\xi,t) - H(-\xi,\xi,t)\right), \tag{1.53}$$

$$\Re\mathrm{e}\tilde{H}(\xi,t) = \mathcal{P}\int_0^1 \left[\tilde{H}(x,\xi,t) + \tilde{H}(-x,\xi,t)\right] C^-(x,\xi)dx, \tag{1.54}$$

$$\Im\mathrm{m}\tilde{H}(\xi,t) = \pi\left(\tilde{H}(\xi,\xi,t) + \tilde{H}(-\xi,\xi,t)\right), \tag{1.55}$$

$$\tag{1.56}$$

where $C^{\pm}$ is :

$$C^{\pm}(x,\xi) = \frac{1}{x-\xi} \pm \frac{1}{x+\xi}\ . \tag{1.57}$$

1.4.3.2 Higher twists and CFF extraction from DVCS

The photon electroproduction cross section depends on the angle ϕ. Mueller and Belitsky performed an harmonic expansion of $|\mathcal{T}_{DVCS}|^2$, $|\mathcal{T}_{BH}|^2$ and $\mathcal{I}$ as a function of ϕ up to twist-3. Since it is central to our analysis, we are going to review this expansion for the unpolarized and beam helicity dependent cross sections. Further details can be found in [17].

1.4.3.2.1 The squared Bethe-Heitler amplitude The Bethe-Heitler process is a pure QED process. Its cross section has been calculated and expressed as a harmonic expansion as a function of ϕ [18]:

$$|\mathcal{T}_{BH}|^2 = \frac{e^6}{y^2 x_B^2[1+4x_B^2M^2/Q^2]^2 t P_1(\phi)P_2(\phi)}\left\{c_0^{BH} + \sum_{n=1}^{2} c_n^{BH}cos(n\phi) + s_1^{BH}sin(\phi)\right\}, \tag{1.58}$$

with

$$J = \left(1-y-\frac{y\epsilon^2}{2}\right)\left(1+\frac{t}{Q^2}\right) - (1-x_B)(2-y)\frac{t}{Q^2}, \tag{1.59}$$

$$P_1(\phi) = -\frac{1}{y(1+\epsilon^2)}\{J + 2K\cos(\phi)\}, \tag{1.60}$$

$$P_2(\phi) = 1 + \frac{t}{Q^2} + \frac{1}{y(1+\epsilon^2)}\{J + 2K\cos(\phi)\}, \tag{1.61}$$

where $y = \frac{\nu}{E}$ and $\epsilon = \frac{2Mx_B}{Q}$. The kinematic coefficients can be found in [18].

1.4.3.2.2 The squared DVCS amplitude The squared DVCS amplitude contribution has been calculated up to twist-3. When performing the harmonic expansion as a function of ϕ, it reads:

$$|\mathcal{T}_{DVCS}|^2 = \frac{e^6}{y^2Q^2}\left\{c_0^{DVCS} + \sum_{n=1}^{2} c_n^{DVCS}cos(n\phi) + \lambda s_n^{DVCS}sin(n\phi)\right\} \tag{1.62}$$

where λ refers to the beam helicity. The c_i^{DVCS} and s_i^{DVCS} coefficients are given by bilinear combinations of CFFs. For example we have:

$$c_0^{DVCS} = 2\frac{2-2y+y^2+\frac{\epsilon^2}{2}y^2}{1+\epsilon^2}\mathcal{C}_{unp}^{DVCS}(\mathcal{F},\mathcal{F}^*), \tag{1.63}$$

$$\mathcal{C}_{unp}^{DVCS}(\mathcal{F},\mathcal{F}^*) = 4(1-x_B)\mathcal{H}\mathcal{H}^* + 4\left(1-x_B+\frac{2Q^2+t}{Q^2+x_Bt}\frac{\epsilon^2}{4}\right)\tilde{\mathcal{H}}\tilde{\mathcal{H}}^* + \cdots \tag{1.64}$$

The different functions contributing to the squared DVCS amplitude for an unpolarized target are listed in the table 1.1.

	Order	**ϕ-dependence**
$\mathcal{C}_{unp}^{DVCS}(\mathcal{F},\mathcal{F}^*)$	twist-2	constant
$\mathcal{C}_{unp}^{DVCS}(\mathcal{F}_{eff},\mathcal{F}_{eff}^*)$	twist-3	constant
$\Re e[\mathcal{C}_{unp}^{DVCS}(\mathcal{F}_{eff},\mathcal{F}^*)]$	twist-3/twist-2	$\cos\phi$
$\Im m[\mathcal{C}_{unp}^{DVCS}(\mathcal{F}_{eff},\mathcal{F}^*)]$	twist-3/twist-2	$\sin\phi$

Table 1.1: GPD content of the DVCS^2 term up to twist-3.

1.4.3.2.3 The interference between the Bethe-Heitler and the DVCS processes

The DVCS squared amplitude is given by bilinear combinations of CFFs. In other words we mainly get information about the modulus of the CFFs. We need information about the phase to extract the CFFs and it cannot be provided by the squared DVCS amplitude. The Bethe-Heitler/DVCS interference term makes the photon electroproduction unique because it is parametrized by the real and imaginary parts of the CFFs. For instance, the unpolarized cross section is sensitive to the real part of $\mathcal{H}$ whereas we extract its imaginary part from the difference of cross sections for opposite beam helicities.

Using the same method as for the squared amplitude of DVCS and BH, we write:

$$I = \frac{\pm e^6}{x_B y^3 t P_1(\phi) P_2(\phi)}\left\{c_0^I + \sum_{n=1}^{3} c_n^I cos(n\phi) + \lambda s_n^I sin(n\phi)\right\}. \tag{1.65}$$

The Fourier coefficient are then given by:

$$c_n^I = C_{++}(n)\ \Re e\mathcal{C}_{++}^I(n|\mathcal{F}) + C_{0+}(n)\ \Re e\mathcal{C}_{0+}^I(n|\mathcal{F}_{eff}), \tag{1.66}$$

$$s_n^I = S_{++}(n)\ \Im m\mathcal{S}_{++}^I(n|\mathcal{F}) + S_{0+}(n)\ \Im m\mathcal{S}_{0+}^I(n|\mathcal{F}_{eff}). \tag{1.67}$$

The $C_{++}(n)$, $S_{++}(n)$, $C_{0+}(n)$ and $S_{0+}(n)$ are only kinematical factors depending on Q^2, t, x_B, ϕ. And $\mathcal{C}_{0+}^I(n|\mathcal{F}_{eff})$ and $\mathcal{C}_{++}^I(n|\mathcal{F})$ are defined such as:

$$\mathcal{C}_{++}^I(n|\mathcal{F}) = \mathcal{C}^I(\mathcal{F}) + \frac{C_{++}^V(n)}{C_{++}(n)}\mathcal{C}^{I,V}(\mathcal{F}) + \frac{C_{++}^A(n)}{C_{++}(n)}\mathcal{C}^{I,A}(\mathcal{F}), \tag{1.68}$$

$$\mathcal{C}_{0+}^I(n|\mathcal{F}_{eff}) = \frac{\sqrt{2}}{2-x_B}\frac{\widetilde{K}}{Q}\Big[\mathcal{C}^I(\mathcal{F}_{eff}) + \frac{C_{0+}^V(n)}{C_{0+}(n)}\mathcal{C}^{I,V}(\mathcal{F}_{eff}) + \frac{C_{0+}^A(n)}{C_{0+}(n)}\mathcal{C}^{I,A}(\mathcal{F}_{eff})\Big], \tag{1.69}$$

Finally, the CFFs are encapsulated in $\mathcal{C}^I$, $\mathcal{C}^{I,V}$, $\mathcal{C}^{I,A}$:

$$\mathcal{C}^I_{unp}(\mathcal{F}) = F_1\mathcal{H} - \frac{t}{4M^2}F_2\mathcal{E} + \frac{x_B}{2 - x_B + x_B\frac{t}{Q^2}}(F_1 + F_2)\widetilde{\mathcal{H}}, \tag{1.70}$$

$$\mathcal{C}^{I,V}_{unp}(\mathcal{F}) = \frac{x_B}{2 - x_B + x_B\frac{t}{Q^2}}(F_1 + F_2)(\mathcal{H} + \mathcal{E}), \tag{1.71}$$

$$\mathcal{C}^{I,A}_{unp}(\mathcal{F}) = \frac{x_B}{2 - x_B + x_B\frac{t}{Q^2}}(F_1 + F_2)\widetilde{\mathcal{H}}. \tag{1.72}$$

We notice that the form factors F_1 and F_2 are associated with the CFFs because they parametrize the Bethe-Heitler process.

	Order	**ϕ-dependence**
$\Re e\ \mathcal{C}^I_{unp}(\mathcal{F})$	twist-2	$\cos\phi$
$\Re e\ \mathcal{C}^{I,V}_{unp}(\mathcal{F})$	"twist-3"	constant
$\Re e\ \mathcal{C}^{I,A}_{unp}(\mathcal{F})$	"twist-3"	$\cos\phi$
$\Re e\ \mathcal{C}^I_{unp}(\mathcal{F}_{eff})$	twist-3	$\cos 2\phi$
$\Im m\ \mathcal{C}^I_{unp}(\mathcal{F})$	twist-2	$\sin\phi$
$\Im m\ \mathcal{C}^{I,V}_{unp}(\mathcal{F})$	"twist-3"	$\sin\phi$
$\Im m\ \mathcal{C}^{I,A}_{unp}(\mathcal{F})$	"twist-3"	$\sin\phi$
$\Im m\ \mathcal{C}^I_{unp}(\mathcal{F}_{eff})$	twist-3	$\sin 2\phi$

Table 1.2: GPD content of the interference term up to twist-3. "twist-3" means *kinematically suppressed like a twist-3*.

1.4.4 Deep π^0 electroproduction

1.4.4.1 Deeply virtual meson production

Deeply virtual meson production is also a key process to study the nucleon. The DVMP cross section can be decomposed into responses according to the polarization states of the virtual photon and their interferences.

$$\frac{d^4\sigma}{dtd\phi dQ^2dx_B} = \frac{1}{2\pi}\Gamma_{\gamma^*}(Q^2, x_B, E_e)\left[\frac{d\sigma_T}{dt} + \epsilon^*\frac{d\sigma_L}{dt} + \sqrt{2\epsilon^*(1+\epsilon^*)}\frac{d\sigma_{TL}}{dt}cos(\phi) + \epsilon^*\frac{d\sigma_{TT}}{dt}cos(2\phi)\right], \tag{1.73}$$

$$\Gamma_{\gamma^*}(Q^2, x_B, E_e) = \frac{\alpha}{8\pi}\frac{Q^2}{M^2E_e^2}\frac{1 - x_B}{x_B^3}\frac{1}{1 - \epsilon^*}, \tag{1.74}$$

$$\epsilon^* = \frac{1 - y - \frac{Q^2}{4E_e^2}}{1 - y + \frac{y^2}{2} + \frac{Q^2}{4E_e^2}}, \tag{1.75}$$

where $\Gamma_{\gamma^*}(Q^2, x_B, E_e)$ represents the flux of virtual photons, and ϵ^* its degree of polarization. σ_L and σ_T are the responses to a photon with longitudinal and tranverse polarizations. σ_{TL} is the interference between the longitudinal and the transverse responses, σ_{TT} the interference between the two transverse polarizations.

Unlike DVCS, the hard part involves strong vertices and an additional non-perturbative object, the distribution amplitude, to describe the structure of the produced meson.

$$\Phi_\pi(x) = \int \frac{dz^-}{2\pi}e^{i(2x-1)P^+\frac{z^-}{2}}\langle\pi, P|\bar{\Psi}\left(-\frac{z}{2}\right)\gamma\cdot n\gamma_5\Psi\left(\frac{z}{2}\right)|0\rangle\big|_{z^+=\vec{z}_\perp=0}. \tag{1.76}$$

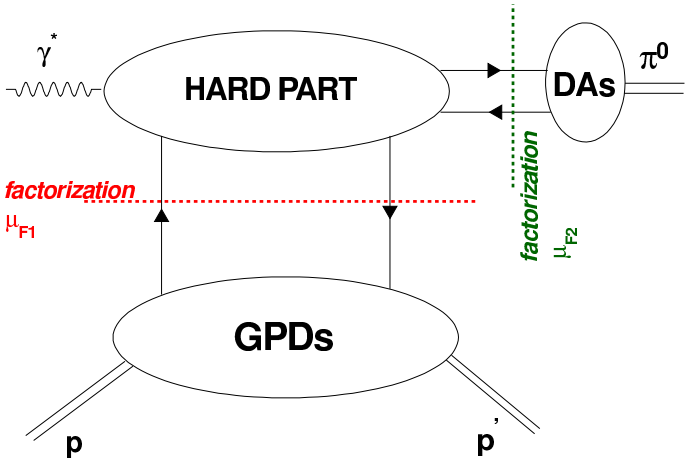

Figure 1.9: Two factorizations are needed to describe π^0 electroproduction with GPDs. The factorization scales μ_{F1} and μ_{F2} are not necessarily equal.

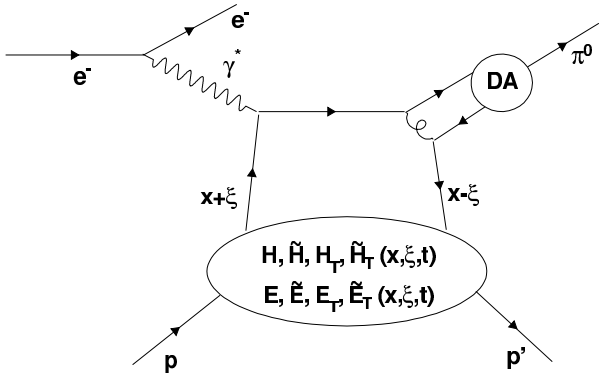

Figure 1.10: One of the diagrams for π^0 electroproduction at leading-twist, leading-order. Unlike DVCS, there are strong vertices in the hard part and one needs to introduce another non-perturbative object called distribution amplitude (DA), which describes the structure of the meson. Note that factorization has been proven only for longitudinally polarized photons.

Because of this additional subtlety, the factorization theorem has been proven only for longitudinally polarized virtual photons. At leading-twist, the longitudinal amplitude involves the unpolarized GPDs H and E for vector mesons, $\tilde{H}$ and $\tilde{E}$ for pseudoscalar mesons. For π^0 at leading-twist and leading-order, the longitudinal amplitude reads:

$$\mathcal{M}^L_{\pi^0} = -ie\frac{4}{9}\frac{1}{\sqrt{Q^2}}4\pi\alpha_S\left[\int_0^1 dz\frac{\Phi_{\pi^0}(z)}{z}\right]\times\frac{1}{2}\int_{-1}^1 dx\left[\frac{1}{x-\xi+i\epsilon}+\frac{1}{x+\xi+i\epsilon}\right]$$
$$\left\{\tilde{H}^p_{\pi^0}(x,\xi,t)\bar{N}(p')\not{n}\gamma^5 N(p)+\frac{\xi}{2M}\tilde{E}^p_{\pi^0}(x,\xi,t)\bar{N}(p')\gamma^5 N(p)\right\}, \quad (1.77)$$

where Φ_{π^0} is the neutral pion twist-2 asymptotic distribution amplitude, $(\tilde{H}^p_{\pi^0},\tilde{E}^p_{\pi^0})$ linear combinations of u/d-GPDs in proton defined such as:

$$\Phi_{\pi^0}(z) = \sqrt{2}f_\pi 6z(1-z), \quad (1.78)$$
$$\tilde{H}^p_{\pi^0}(x,\xi,t) = \frac{1}{\sqrt{2}}\left\{\frac{2}{3}\tilde{H}^{u/p}_{\pi^0}-\left(-\frac{1}{3}\right)\tilde{H}^{d/p}_{\pi^0}\right\}, \quad (1.79)$$
$$\tilde{E}^p_{\pi^0}(x,\xi,t) = \frac{1}{\sqrt{2}}\left\{\frac{2}{3}\tilde{E}^{u/p}_{\pi^0}-\left(-\frac{1}{3}\right)\tilde{E}^{d/p}_{\pi^0}\right\}, \quad (1.80)$$

with f_π=0.0924 GeV and $z=(p\cdot q')/(p\cdot q)$.

Using models of $\tilde{H}$ and $\tilde{E}$ adjusted on DVCS data, the longitudinal response for π^0 electroproduction is expected to be small.

1.4.4.2 Beyond leading-twist: Twist-3 DA and transversity GPDs

Although factorization has not yet been proven for transverse virtual photons in DVMP, Goloskokov *et al.* have elaborated a model [19][20] involving the transversity GPDs. As the transversity GPDs are chiral-odd, they cannot couple to the twist-2 DA of the pion which is chiral-even. Chiral-odd DAs appear at twist-3 when considering the transverse momentum of the quark entering the meson, with respect to the meson momentum. Although the twist-3 contributions are kinematically suppressed with respect to twist-2 ones, the twist-3 DAs include a factor $\mu_\pi=\frac{m_\pi^2}{m_u+m_d}$ (with m_u and m_d are the bare quark masses) which does not appear in the twist-2 DA. As a consequence, this factor boosts the transverse response and significantly increases the π^0 electroproduction cross section. It is interesting to note that, within this model, we can directly access the information on H_T, $\tilde{H}_T$ and E_T by measuring σ_T and σ_{TT}.

$$\frac{d\sigma_T}{dt} = \frac{4\pi\alpha}{2k'}\frac{\mu_\pi^2}{Q^8}\left[(1-\xi^2)|\langle H_T\rangle|^2-\frac{t'}{8m^2}|\langle 2\tilde{H}_T+E_T\rangle|^2\right], \quad (1.81)$$
$$\frac{d\sigma_{TT}}{dt} = \frac{4\pi\alpha}{2k'}\frac{\mu_\pi^2}{Q^8}\frac{t'}{16m^2}|\langle 2\tilde{H}_T+E_T\rangle|^2, \quad (1.82)$$

where k' is a phase space factor given by:

$$k' = \frac{16\pi}{Q^2}\left(\frac{1}{x_B}-1\right)\sqrt{(W^2-m^2)^2+Q^4+2W^2Q^2+2Q^2m^2}\,. \quad (1.83)$$

Finally $\langle F\rangle$ stands for the following convolution of a GPD F with the hard scattering kernel $\mathcal{D}_{\mu'\lambda'\mu\lambda}$ summed over the incoming quark helicity λ.

$$\langle F\rangle = \sum_\lambda\int_{-1}^1 dx\mathcal{D}_{\mu'\lambda'\mu\lambda}F, \quad (1.84)$$

λ, λ' are the helicity of the incoming and outgoing quarks, μ the helicity of the incident electron. μ' is the helicity of the produced meson which is 0 for pseudo-scalar mesons.

1.5 Experimental status

1.5.1 DVCS results

A worldwide experimental program has been developed in order to measure DVCS observables in different kinematical regions (Figure 1.11). In this review, we are not going to talk about the Jefferson Lab-Hall A experiments since they are the topic of this thesis.

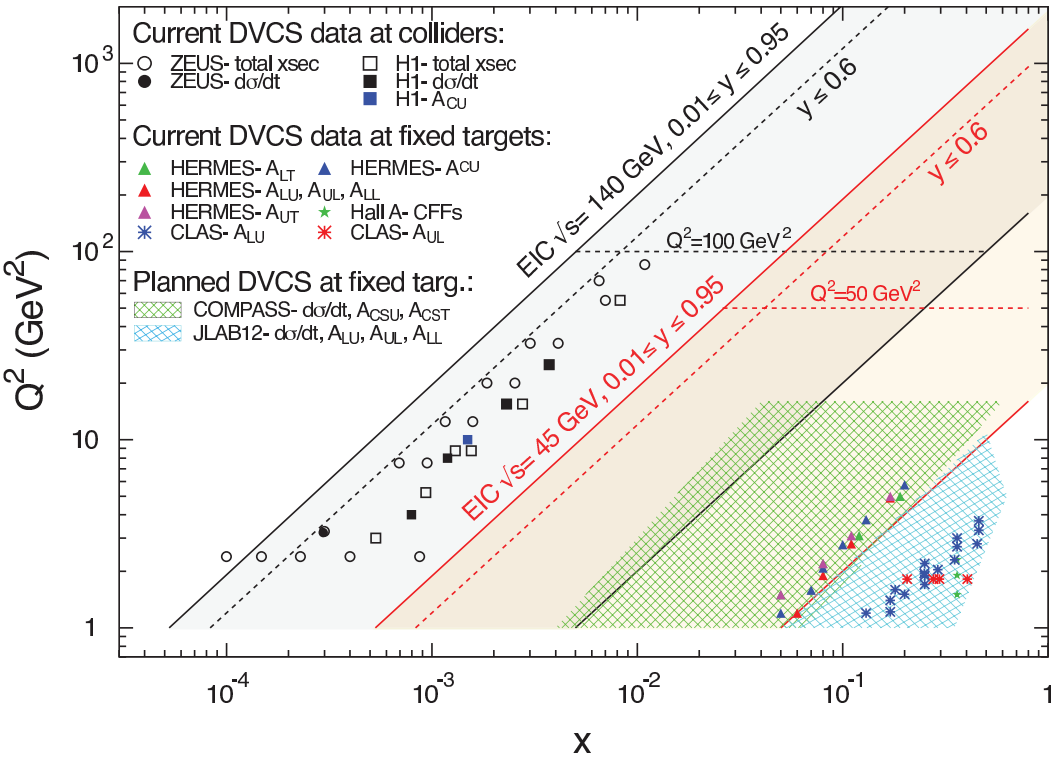

Figure 1.11: Q^2 versus x_B for the past and future experiments [21]. Unpolarized and beam-helicity dependent cross sections have recently published by the CLAS [22] and Hall A [23] collaborations.

1.5.1.1 H1 and ZEUS

The H1 and ZEUS experiments were located at DESY laboratory in Hamburg, Germany and ran until 2007. They were collider experiments between an electron/positron beam and a proton beam provided by the HERA (Hadron-Elektron-Ring-Anlage) accelerator. H1 and ZEUS measured total ([24][25]) and t-differential ([26][27]) cross sections for Q^2 up to 25 GeV^2 and W up to 100 GeV. Thanks to the ability to use both electrons and positrons, the H1 collaboration also extracted beam charge asymmetries [28].

The factorization of the cross section and the dominance of gluon GPDs at low x_B were demonstrated with these data.

1.5.1.2 HERMES

The HERMES spectrometer also installed on the HERA accelerator was a fixed target experiment using an internal gaseous target. The HERMES collaboration measured DVCS

observables in the Q^2 range from 1 to ∼6 GeV^2 and x_B from 0.04 to 0.2. For the first measurements, exclusivity was ensured by a missing-mass cut $M^2_{ep\to e\gamma X}$. For the last run period until June 2007, a recoil detector was added to the spectrometer in order to reduce systematic errors related to exclusivity [29].

The target could be polarized both longitudinally and transversely. Combining the target and beam polarizations, using electron and positrons, HERMES measured an almost complete set of asymmetries, but no cross sections. This very complete set of observables is a convenient way to unfold the different CFF contributions [30][31][32] (see section 1.4.3.2).

1.5.1.3 JLab-CLAS results

CLAS (*CEBAF large acceptance spectrometer*) is installed in the Hall B of Jefferson Laboratory in Virginia, USA. As its name indicates, CLAS covers a large solid angle, compared to Hall A for instance, albeit at a reduced luminosity. The CLAS collaboration measured DVCS observables over a wide range in Q^2 (between 1 and ∼4.8 GeV^2) and x_B (between 0.1 to almost 0.6). The longitudinally polarized electron beam from the accelerator interacts with a liquid hydrogen target to study beam spin asymmetries [33]. Later, data on longitudinally polarized NH_3 target were taken to extract target spin [34] and double spin asymmetries [35]. Very recently, the CLAS collaboration released unpolarized and beam-helicity-dependent cross sections [22].

Within their statistical accuracy, HERMES and CLAS data are well described by leading-twist predictions. Note that there is a disagreement between CLAS and HERMES data concerning the $\sin 2\phi$ harmonic of the asymmetry unpolarized beam on a longitudinally polarized target (A_{UL}): whereas CLAS find a result compatible with 0, HERMES finds a sizeable $\sin 2\phi$ harmonics which cannot be reproduced by only considering the leading-twist contribution [36].

1.5.1.4 Future experiments

As seen on figure 1.11, available data are spread over a large kinematic area but there are some domain with no data:

- A large area between x_B=10^{-3} and x_B=10^{-2} where no data are available yet. But in 2016, the Common Muon and Proton Apparatus for Structure and Spectroscopy (COMPASS) experiment will measure DVCS cross sections in this region, connecting the fixed target domain to the high energy collider one. A 160 GeV muon beam interacts with a 2 m-long liquid hydrogen target. A recoil detector, CAMERA, detects the proton. The photon will be detected in a set of three calorimeters. The scattered muon will be detected in the standard COMPASS spectrometer.

- The high x_B-region suffers from a lack of statistically significant data. Nevertheless the upgrade of CEBAF to 12 GeV allows for high accuracy experiments in this kinematical region. In particular, a dedicated experiment started in Hall A at the end of 2014. After the CLAS spectrometer is upgraded with a new detector package and new magnets, a number of experiments will also take data in this enlarged kinematical domain. Finally, Hall C of Jefferson Laboratory will perform the Rosenbltuh separation of photon and π^0 electroproduction cross sections around 2020, accessing higher Q^2 and x_B values thanks to the High Momentum Spectrometer.

- Last but not least, it is the strong desire of the hadronic physics community worldwide to build the ultimate accelerator in order to study nucleon structure: The Electron-Ion Collider (EIC) will use intense and polarized beams of electrons and ions in order

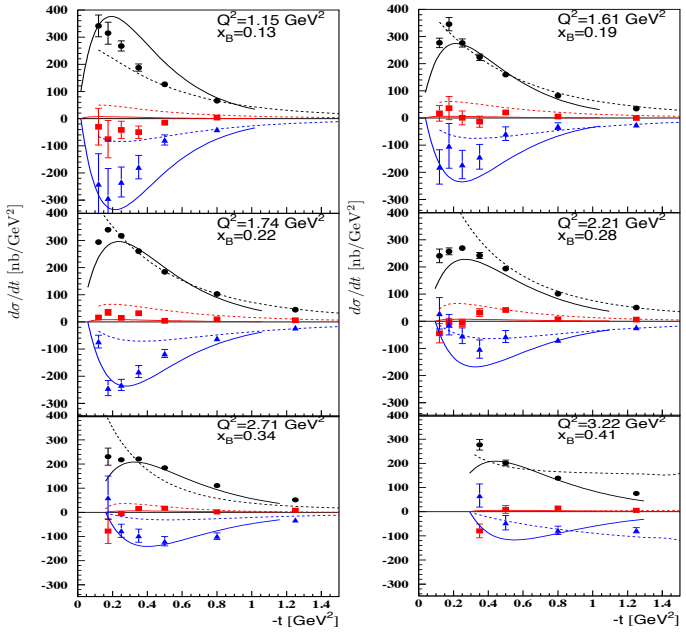

Figure 1.12: $\sigma_T + \epsilon^* \sigma_L$ (back points), σ_{TT} (blue points) and σ_{TL} (red points) extracted by the CLAS collaboration [38]. The solid curves represent Goloskokov and Kroll's model [20], able to reproduce the behaviour of the cross sections. The dashed lines represent prediction of the model developed by Goldstein and Liuti [39].

to study gluon-dominated matter. In particular, the ability to transversally polarize protons will help tremendously to pinpoint the elusive GPD E.

1.5.2 Pion electroproduction data

Measurements of pion electroproduction cross sections have been carried out in the different JLab experimental hall. We focus on the unpolarized cross section results of π^0. We also dedicate a section to the Rosenbluth separation performed on the π^+ electroproduction.

1.5.2.1 π^0 electroproduction data

Two experiments have measured π^0 electroproduction cross sections in the valence region. First results were published by the Hall A collaboration [37]. These measurements have then been extended in a wider kinematical range by the CLAS collaboration [38] (Figure 1.12). Whereas σ_L is expected small by twist-2 GPD models, both experiments measured high unpolarized cross sections potentially indicating a large transverse contribution.

The large transverse-transverse interference term σ_{TT} also supports the assumption of a large σ_T-contribution.

1.5.2.2 Rosenbluth separation on π^+ electroproduction cross section

A L/T separation has been performed on $ep \to en\pi^+$ in the Hall C of Jefferson Lab [40]. The longitudinal and transverse contributions have both been found significant (Figure 1.13), even at high Q^2, whereas the transverse response is supposed to be suppressed by $1/Q^2$ with respect to the longitudinal one. Although σ_L is expected to be small for π^0, it is enhanced in the case of π^+ by an additional channel. This channel consists of an exchange of a virtual

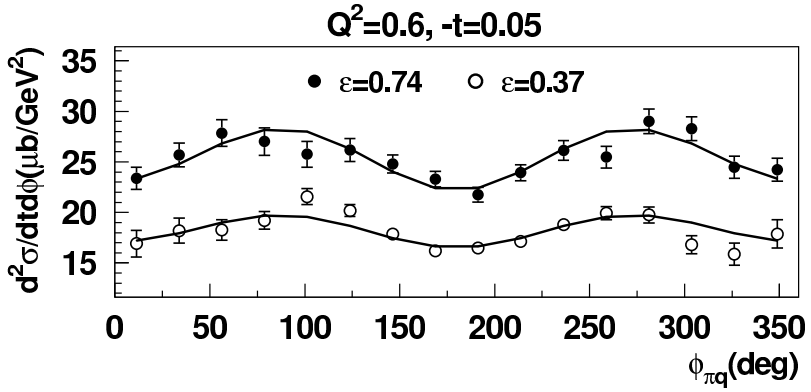

Figure 1.13: $\gamma^* p \to n\pi^+$ extracted at two ϵ^*'s values [41]. Because σ_L and $\Delta\epsilon$ are important, the cross section has increased significantly.

π^+ between the virtual photon and the nucleon. It can be seen as virtual photon scattering off the pion cloud in the proton. As a consequence, the associated amplitude has $(t - m_\pi)$ in its denominator, coming from the pion propagator, enhancing the longitudinal response. Finally, the Q^2-dependence of σ_L was in agreement with the model whereas σ_T was found to scale down much slower than the expected $\frac{1}{Q^8}$.

1.6 The E00-110 and E07-007 experiments

In this thesis, we will describe and analyze two experiments which ran in the Hall A of Jefferson Lab. We may consider them as two run periods of a same experiment. They both studied photon and π^0 electroproduction. We first introduce the 2004 [42] and then the 2010 [43] run periods.

1.6.1 The E00-110 experiment: the 2004 run period

The first run period was in 2004. Its purpose was to perform a Q^2-scan at fixed x_B of the beam helicity dependent DVCS cross section to test the scaling of DVCS [44]. The kinematical settings are listed in Table 1.3. In addition, an extra set of unpolarized cross sections for the kinematics with the highest value of Q^2 was extracted. Indeed it was possible to evaluate the π^0 contamination (explained later in the thesis) for the highest Q^2 setting, hinting that π^0 electroproduction could be extracted.

Setting	k' (GeV/c)	θ_e (°)	Q^2 (GeV^2)	x_B	θ_q (°)	W (GeV)	E_γ (GeV)
2004-Kin1	3.53	15.6	1.5	0.36	−22.3	1.9	2.14
2004-Kin2	2.94	19.3	1.9	0.36	−18.3	2.0	2.73
2004-Kin3	2.34	23.8	2.3	0.36	−14.8	2.2	3.32

Table 1.3: Experimental $ep \to ep\gamma$ kinematics, for incident beam energy $E_b = 5.7572$ GeV. θ_q is the central value of the **q**-vector direction. E_γ is the photon energy for $t = t_{\min}$. Note that only the average kinematic values for each setting are listed in this table : in order to minimize systematic bin centering effects, we actually used the kinematic of each bin in x_B, Q^2 and t according to their average value in the bin.

A CFF extraction was performed on the polarized and unpolarized results. From the polarized cross section, hints of scaling was found since the extracted combinations of CFFs

showed no Q^2-dependence (Figure 1.14). Assuming a negligible contribution of $|\mathcal{T}_{DVCS}|^2$, the three lowest twist CFFs parametrizing the interference contribution have been extracted using the unpolarized data. However, the large size of the extracted interference terms raised doubts concerning the hypothesis of a negligible $|\mathcal{T}_{DVCS}|^2$.

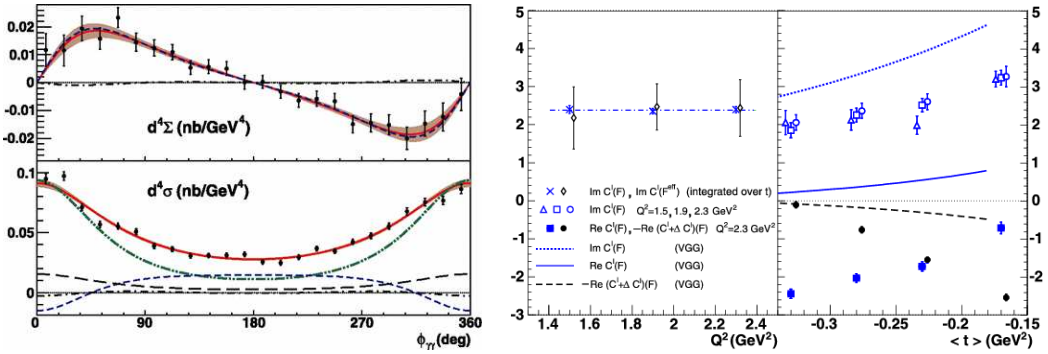

Figure 1.14: Left: Beam helicity dependent and unpolarized photon electroproduction cross sections at $t = -0.28$ GeV^2, $Q^2 = 2.3$ GeV^2 and $x_B = 0.36$ from [44]. Right: Compton form factors extracted from the 2004 experiment, assuming a negligible $DVCS^2$ contribution.

From the same run period, π^0 electroproduction cross sections have been extracted [37]. Almost instantly, π^0's decay into two photons with a branching ratio of 98.8%. As this experiment was suited to detect the photon in the DVCS process, it was sensitive to π^0's through the decay photons. However the threshold set on the energy of the photon at ~ 1 GeV reduced the phase space of the π^0 detection, possible only with 2-photon detection. As the π^0 energy decreases with decreasing Q^2, this phase space was too small for 2004-Kin1 to extract π^0 electroproduction cross section. However it was large enough for 2004-Kin3 and 2004-Kin2 [37]. They also studied the x_B-dependence by defining new kinematics from the 2004-Kin2 and 2004-Kin3 data set.

An interesting point is that π^0 electroproduction cross sections have been extracted for 2004-Kin2. It implies that the π^0 contamination can be estimated for 2004-Kin2 data. A chapter of this thesis is dedicated to the full reanalysis of DVCS data from the E00-110 experiment.

1.6.2 The E07-007 experiment: the 2010 run period

The conclusion of the 2004 run period was that both photon and π^0 electroproduction unpolarized cross sections were higher than predicted. But we did not know the size of the different contributions, nor did we understand the discrepancy with the predictions. It was the goal of the 2010 experiment to perform a complete separation of photon and π^0 electroproductions. Similarly to 2004, the goal of the 2010 run period was to extract DVCS and π^0 electroproduction cross section but at two different beam energies E for each kinematical setting (Table 1.4). The idea is to combine the dependences in ϕ and E to disentangle all contributions. Indeed the kinematical factors in front of the dominant terms of interference and $DVCS^2$ do not depend on ϕ but have different beam energy dependences (see the tables 1.1 and 1.2). For π^0, as shown explicitely in Eq 1.73, we have to measure the cross section at two different values of ϵ^* in order to disentangle the transverse and the longitudinal responses.

The experiment ran from October to December 2010, at the same time as the Q-weak experiment in Hall C. Because of constraints on the beam energy due to Q-weak, kinematics were slightly different compared to the E00-110 experiment.

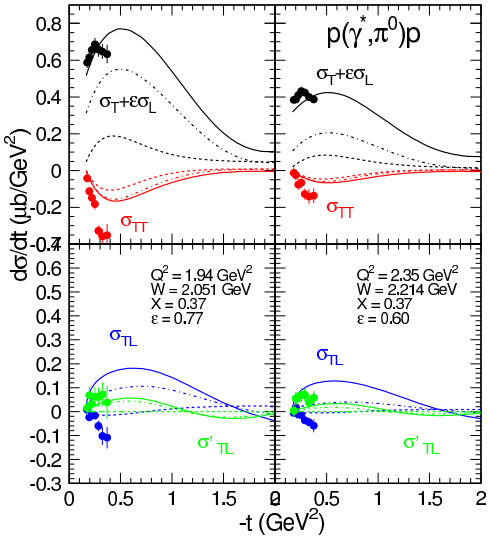

Figure 1.15: Results of π^0 electroproduction from Hall A [37]. The lines represent predictions based on t-channel meson exchange [45].

Name	Q^2 (GeV^2)	x_B	W^2 (GeV^2)	E (GeV)	ϵ^*
2010-Kin1	1.5	0.36	3.55	(3.355 ; 5.55)	(0.52 ; 0.84)
2010-Kin2	1.75	0.36	3.99	(4.455 ; 5.55)	(0.65 ; 0.79)
2010-Kin3	2	0.36	4.44	(4.455 ; 5.55)	(0.53 ; 0.72)

Table 1.4: Table of kinematics for the 2010 experiment.

As explained in section 1.4.4, σ_L is expected to be very small and the lever arm in ϵ^* is rather small. It makes this measurement a technical challenge, with a dire need to reduce as much as possible the systematic uncertainties.

Chapter 2

The experimental setup

Jefferson laboratory is located in Newport News (Virginia, USA) and was founded in 1985. Its primary mission is to investigate the structure of nuclei and nucleons. To accomplish this mission, a continuous electron beam accelerator facility (CEBAF) has been built and has provided a longitudinally polarized electron beam to three experimental halls since 1995. Both experiments of interest in this thesis took place in the Hall A of Jefferson laboratory, dedicated to high luminosity and high precision experiments. Except for a few details which will be presented in their dedicated chapters, the E07-007 and E00-110 experiments are identical.

First, we are going to introduce CEBAF and then the Hall A of Jefferson Lab. We will then describe the experimental setup of both experiments.

2.1 Continuous electron beam accelerator facility

The electron source is a stressed gallium arsenide crystal, placed in an ultra-vacuum chamber. Using optical pumping, the conduction band of the crystal is filled with electrons from the valence band [46]. By choosing the polarization of the pumping laser, we can choose the polarization state of the electrons in the conduction band. To increase the probability for the electron to go in the vacuum, a layer of cesium fluoride is deposited at the interface to lower the potential barrier between the vacuum and the conduction band. Once the electron escapes from the crystal, a difference of potential extracts it. Instead of a unique laser illuminating the GaAs cathode, there are three lasers functionning at 499 Mhz each. Each experimental hall is synchronized with its own laser.

Until 2014, CEBAF was composed of two superconducting linacs made of 20 cryomodules, each cryomodule composed of 8 radio-frequency cavities in pure Niobium (see Figure 2.1). The electromagnetic magnetic field in the cavities is a stationary sinusoidal field synchronized with the injector (1497 MHz). The resulting increase for each cavity in energy is $\sim$7 MeV/m. The two linacs were connected by recirculating arcs allowing to reinject the beam 5 times in each linac for a maximal beam energy of $\sim$6 GeV. To avoid the spatial spread of the electron bunches, the electrons from the source have to be accelerated by a first set of cavities up to 45 MeV before entering the linacs. Using RF separators and magnets, the beam is then sent in the 3 experimental Halls. Hall A and C could receive up to 150 μA of beam current, whereas Hall B was limited to 200 nA.